

Journal of Thermal Stresses

ISSN: 0149-5739 (Print) 1521-074X (Online) Journal homepage: www.tandfonline.com/journals/uths20

Heat and mass transfer impact on magnetized chemically reactive sodium alginate flow in porous structures for nanotechnology applications

U. S. Mahabaleshwar, S. M. Sachhin, G. M. Sachin, S. W. Joo, U. Guevara & L. M. Pérez

To cite this article: U. S. Mahabaleshwar, S. M. Sachhin, G. M. Sachin, S. W. Joo, U. Guevara & L. M. Pérez (27 Oct 2026): Heat and mass transfer impact on magnetized chemically reactive sodium alginate flow in porous structures for nanotechnology applications, Journal of Thermal Stresses, DOI: 10.1080/01495739.2026.2743583

To link to this article: https://doi.org/10.1080/01495739.2026.2743583

Published online: 27 Oct 2026.

Submit your article to this journal

Article views: 20

View related articles

View Crossmark data

Full Terms & Conditions of access and use can be found at
https://www.tandfonline.com/action/journalInformation?journalCode=uths20

JOURNAL OF THERMAL STRESSES
https://doi.org/10.1080/01495739.2026.2743583

Taylor & Francis
by informa

Check for updates

Heat and mass transfer impact on magnetized chemically reactive sodium alginate flow in porous structures for nanotechnology applications

U. S. Mahabaleshwar[a], S. M. Sachhin[b], G. M. Sachin[a], S. W. Joo[c], U. Guevara[d], and L. M. Pérez[e]

[a]Department of Studies in Mathematics, Davangere University, Davangere, India; [b]Department of Mathematics and Statistics, M S Ramaiah University of Applied Sciences, Bangalore, India; [c]Department of Mechanical and Automotive Engineering, BIC, Tongmyong University, Busan, Korea; [d]Vicerrectoría de Investigación y Postgrado, Universidad de La Serena, La Serena, Chile; [e]Departamento de Ingeniería Industrial y de Sistemas, Universidad de Tarapacá, Arica, Chile

ABSTRACT

The current article aims to determine the influence of porous media and engineering quantities on chemically reactive magnetic sodium alginate fluid flow with entropy generation examination. It is noted that there is a dearth of investigation on chemically reactive magnetic sodium alginate fluids under the circumstances of MHD, porous media, radiation, heat source, and chemical reaction. The authors addressed this research gap. Nonlinear governing equations scrutinized to ODEs by utilizing similarity terms, heat source/sink, and solar radiation effects were added in the energy equation, then formulated by the Laguerre polynomials series approach, and also studied the irreversibility of processes functionality, findings of the present analysis illustrate that increasing the magnetic field decreases the momentum of the fluid and increases the temperature by 19%; raising the thermal radiation upsurges the temperature. The rate of heat transmission is enhanced by 22% when the heat source increases from 1 to 4, and heat transmission increases by 28% when the thermal radiation increases from 1 to 4. Bingham fluids are beneficial in situations requiring controlled flow, such as the transfer of sewage, where the yield stress may prevent leakage by blocking flow under low force. And also employed in cooling systems for electrical devices and transformers, which require excellent heat dissipation.

HIGHLIGHTS

- The current article aims to study the impact of engineering quantities on fluid flow.
- Nonlinear governing equations scrutinized to ordinary differential equations.
- dissipation and joule heating effects added to the temperature equation.
- Al_2O_3 and SiO_2 nanoparticles form hybrid nanofluids in sodium alginate.
- Studied the entropy generation and chemical reaction in the fluid flow.

ARTICLE HISTORY
Received 15 November 2025
Accepted 29 September 2026

KEYWORDS
Bi-viscous Bingham fluid; chemical reaction; entropy generation; mass transfer; porous media

1. Introduction

In this modern era, Bingham fluids are used in many industries due to their unique flow properties, characterized by their yield stress and plastic viscosity, which have significant implications in

CONTACT S. M. Sachhin sachinsm030@gmail.com Department of Mathematics and Statistics, Faculty of Natural Sciences, M S Ramaiah University of Applied Sciences, Ramaiah Technology Campus, 4th Phase, Peenya, Bangalore, 560058, Karnataka, India.

© 2026 Taylor & Francis Group, LLC

several industrial processes. Bingham fluids, in contrast to Newtonian fluids. The fluid behaves like a Newtonian liquid with a linear relationship between shear stress and shear rate until the yield stress is surpassed. Because of their dual nature, Bingham fluids are beneficial in situations requiring controlled flow, such as the transfer of sewage, where the yield stress may prevent leakage by blocking flow under low force and enabling it when pushed with sufficient force. Sachhin [1] explored the effect of magnetic attraction on Bingham fluid flows across a permeable barrier. Ajithkumar [2] studied the mixed peristaltic circulation of Bingham tiny fluids *via* a porous material with nonlinear boundary circumstances. Sultan [3] investigated the flow mechanics in a diseased passage of nano-Bingham fluid [4, 5]. studied the theoretical effects of mass flow on magnetic Bingham fluid. Eldabe [6] studied the effect of pressure on the flow of Newtonian tiny fluids with mass and heat exchange.

Many industrial and natural processes rely on chemical reactions in fluid movement. These reactions help in product synthesis, material purification, and pollutant removal in industries such as water treatment, petrochemicals, and pharmaceuticals. For example, chemical reactions in fluid flow in catalytic converters reduce hazardous emissions from vehicles. These activities are vital for nutrient cycling and maintaining ecological equilibrium in natural systems such as rivers and oceans. Understanding and controlling these reactions allows for more effective and long-lasting processes. Shah [7] studied the heat exchange characteristics over the surface of a magnetohydrodynamic fluid movement under the impact of bioconvection. The RKF4th order method was used by Joshi [8] to study the magnetic hybrid fluid flow across a bidirectional permeable surface with volumetric heat generation. Roy [9] studied the impacts of binary chemical reactions on fluid over a permeable stretching sheet. Buongiorno's model was used by Ahmed [10] to study the magnetic boundary layer hybrid nanoliquid movement with chemical reaction. Thermal science and bioengineering applications of hybrid nanofluids studied by Li [11]. Krechetnikov [12] studied the thermal conductivity in human blood vessels with the implementation of a chemical reaction. Fluid flow research and applications in disciplines like engineering and physics rely largely on electromagnetic fields. One notable use is magnetohydrodynamics (MHD), in which magnetic fields influence the behavior of electrically conducting liquids such as plasmas. This has applications in astronomical occurrences such as solar flares and planetary magnetospheres. Electromagnetic fields are vital for fluid flow and have applications in medicine as well. Magnetic resonance imaging (MRI) incorporates principles such as fluid flow and electromagnetic fields to give comprehensive images of the human body. Electromagnetic fields are important in fluid flow research and applications.

Kolin [13] studied the induced electromotive force on the polarized electrode through the wall of the tube. Kuwahara [14] studied the electromagnetic effect on fluid flow by using the optical visualization method. Yu [15] studied the mathematical model of the impacts of the metal droplets' fluid flow. Natarajan [16] studied the three-dimensional electromagnetically driven flow based on integral formulation. Chamkha [17] explored the impacts of electromagnetic stirring and element transport on the thermofluidic movement experimentally. an analytical approach was used by Li [18] to study the electromagnetic levitation processes and magnetohydrodynamic phenomena on the constant eddy viscosity model.

In thermodynamics and fluid mechanics, entropy generation in fluid flow is a crucial topic because it enables us to understand the irreversibility of processes. Irreversible behavior is frequently caused by heat transfer, friction, and viscous dissipation. Applications for the study of entropy creation include the design of heat exchanger optimization, increasing thermal systems' energy efficiency, and enhancing electronic cooling systems' functionality. Through the assessment of entropy generation, engineers may identify areas of energy loss and develop strategies to mitigate them, ultimately leading to the development of more sustainable and effective systems. Ibanez [19] studied the entropy generation analysis of electrical fluid flow over a microchannel under convective boundary conditions. The analytical approach utilized by Zhang [20] to study

the entropy generation and correlations of nanofluid flow over a circular tube [21–24]. explored the thermal radiation and heat absorption effects on viscous fluid.

Hybrid nanofluids are used in solar collectors and photovoltaic systems to increase efficiency by improving heat absorption and transmission. They are also employed in cooling systems for electrical devices, transformers, and engines, which require excellent heat dissipation. Applications of hybrid nanofluids can also be found in medical therapy, such as targeted medication administration and hyperthermia treatment, due to their improved thermal characteristics. These varied uses illustrate hybrid nanofluid's potential to advance technology and improve energy efficiency. The heat flux model was utilized by Dawar [25, 26] to study the heat exchange of a hybrid fluid with sodium alginate. Xue and Yamada-Ota model utilized by Upreti [27] to examine the heat exchange influence on the fluid flow. Li [28] studied the activation energy effect on sodium nanofluids *via* a porous medium with a magnetic field environment [29, 30]. studied the Darcy-Forchheimer model of Williamson fluid flow,

The study of porous media is necessary for many applications involving fluid flow. Water moves *via* the interconnected pores of geological formations, which is why they are essential for hydrogeology's groundwater extraction and aquifer replenishment applications. To boost recovery rates and extract hydrocarbons from reservoirs, the oil and gas industry uses porous medium. In environmental engineering, porous media are also helpful for storing hazardous waste and treating contaminated groundwater. Porous media are also employed in filtration systems to enhance the purification of liquids and gases. These uses demonstrate the diversity and importance of porous media in controlling and taking advantage of fluid flow in several sectors. Wang [31] studied the double-diffusive convection influence on nanofluid flow across a porous surface. Aly [32] studied the Marangoni boundary layer flow of a water-based nanofluid [33–59]. studied the boundary-layer flow within a complex preamble zone over various boundaries.

1.1. Motivation and novelty

Motivated by the above-mentioned research and applications, the current study examines the entropy generation and engineering quantities effect on chemically reactive magnetic sodium alginate fluid flow with mass transfer. It is noted that there is a lack of examination on chemically reactive magnetic sodium alginate fluids in the circumstances of magnetic field porous media and chemical reaction on hybrid nanofluid flow. The study simultaneously incorporates thermal radiation, internal heat generation/absorption, velocity slip, mass transpiration, and chemical reaction effects along with entropy generation analysis. Similarity transformation is used to reduce the governing equations of the problem into a system of nonlinear ordinary differential equations. Energy and concentration equations are solved by using Laguerre polynomials and discussed results of many physical parameters through graphs. Present analysis has many useful applications. Bingham fluids are beneficial in situations requiring controlled flow, such as the transfer of sewage, where the yield stress may prevent leakage by blocking flow under low force. And also employed in cooling systems for electrical devices, transformers, and engines, which require excellent heat dissipation.

1.2. Practical significance of the present physical model

Sodium alginate is a biocompatible, biodegradable, and electrically conducting polymer which finds broad application in biomedical engineering, food processing, pharmaceutical formulations, and also thermal management systems. When sodium alginate is dispersed with nanoparticles, hybrid nanofluids with improved thermal conductivity, stability, and controllable rheological behavior can be obtained. The addition of magnetohydrodynamic effects, porous media, thermal radiation, velocity slip, and chemical reaction in the model simultaneously represents the real

scenario of the advanced engineering applications. Take, for example, magnetic fields which make it possible to direct remotely alginate-based drug delivery systems in targeted therapy. Also, porous structures are naturally occurring in biological tissues, catalytic beds, and heat exchangers. Moreover, the velocity slip effect is relevant to micro- and nano-scale flows, while chemical reactions take place in biochemical processes, environmental remediation, and industrial reactors. Therefore, the study of these combined influences brought together in the model is a smart initiative toward the thorough understanding needed for the optimal design of next generation thermal, biomedical, and energy systems.

1.1. The following section addresses the research gaps

- Examined the analysis of entropy generation.
- Thermal radiation, heat absorption, and viscous dissipation terms are considered in the energy profile.
- Chemical reaction effect incorporated in the mass transfer.
- The percentage upsurge in the physical quantities due to the hybrid nanoparticles is compared to hybrid and single nanoparticles in Sodium Alginate hybrid nanofluid with velocity slip boundary conditions.

1.2. Research questions addressed by the current research

- How do variations in the stretching parameter influence the fluid momentum and viscosity-driven resistance in a reactive magnetic sodium alginate flow?
- How does thermal radiation influence entropy generation and temperature variation, and what implications does this have for thermal control in engineered systems?
- How does internal heat generation, modeled as a heat source/sink term, affect thermal gradients and heat transfer rates, particularly the Nusselt number?
- What impact does the Eckert number have on thermal behavior and entropy production in a chemically reactive and radiatively heated magneto-fluidic environment?
- What is the effect of increasing porosity on the velocity distribution and skin friction in porous media subjected to magneto-hydrodynamic and reactive flow conditions?

2. Physical model with derivation

Considered steady incompressible 2-dimensional flow of Sodium alginate hybrid nanofluid across a penetrable surface, flow takes place at $y \geq 0$, which is normal to the surface, considering sodium alginate as base fluid and Al_2O_3 and SiO_2 tiny particles to form hybrid nanofluid, heat absorption, and solar radiation considered in energy equation, to enhance electronic cooling system's functionality studied the entropy generation, T and C are heat and concentration profiles. Schematic representation shown in Figure 1.

2.1. Limitations and assumptions of the current analysis:

- The fluid viscosity is dependent on the shear rate; Hence, we assumed non-Newtonian fluid.
- Considered incompressible hybrid nanofluid that is non-Newtonian and laminar flow.
- Considered a magnetically conducting sheet.
- Taken hybrid nanofluid as base fluid SA with Al_2O_3, and SiO_2 nanoparticles.
- Joule heating takes place uniformly throughout the surface of the fluid.
- Pressure gradient. i.e., $\nabla p = 0$.

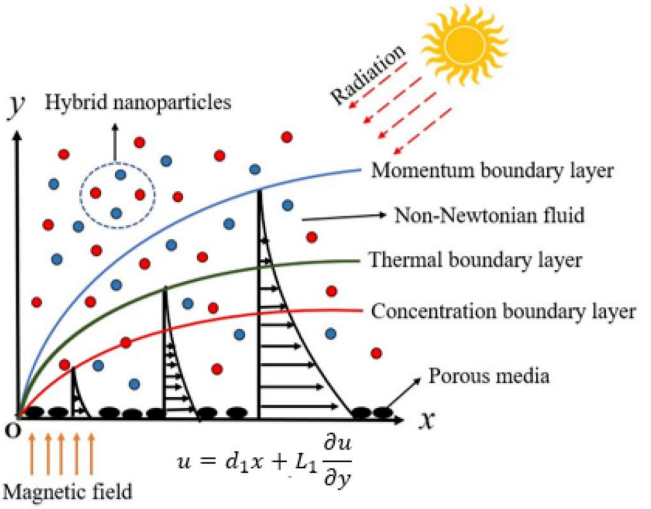


Figure 1. Physical representation.

- Considered velocity slip boundary conditions for the fluid flow.
- Assumed incompressible steady state flow, i.e., $\frac{\partial u}{\partial t} = 0$.

Biviscous Bingham fluid's rheological expression obtained as [26].

$$\tau_{ij} = \begin{cases} 2\left(\mu_B + p_y/\sqrt{2\pi}\right)e_{ij}, \pi > \pi_c, \\ 2\left(\mu_B + p_y/\sqrt{2\pi_c}\right)e_{ij}, \pi < \pi_c, \end{cases} \tag{1}$$

where $P_y = \frac{\mu_B\sqrt{2\pi_c}}{\lambda}$.

2.2. Physical description [1, 15, 26]

2.2.1. Conservation of mass equation [34, 38]

$$\nabla.\vec{q} = 0.$$

The conservation velocity is written as [34, 39, 42].

$$\left[\left(\vec{q} \bullet \nabla\right)\vec{q}\right] = \left(1 + \frac{1}{\lambda}\right)\frac{\mu_{hnf}}{\rho_{hnf}}\nabla^2\vec{q} - \frac{\mu_{hnf}}{\rho_{hnf}K*}\vec{q} - \frac{\sigma_{hnf}}{\rho_{hnf}}B_0^2\vec{q}, \tag{2}$$

the conservation energy equation [34, 39, 42].

$$(\rho Cp)_{hnf}\left(\vec{q} \bullet \nabla\right)T = \kappa_{hnf}\nabla^2 T - \nabla \cdot q_r + Q_0(T - T_\infty) + \mu_{hnf}\Phi + \sigma_{hnf}B_0^2\left|\vec{q}\right|^2, \tag{3}$$

the conservation concentration equation [39, 42].

$$\left(\vec{q} \bullet \nabla\right)C = D_b\nabla^2 C - Cr^*(C - C_\infty).[] \tag{4}$$

Governing equations are generally written as [1, 15, 26].

$$\frac{\partial u}{\partial x} + \frac{\partial v}{\partial y} = 0, \tag{5}$$

$$u\frac{\partial u}{\partial x}+v\frac{\partial u}{\partial y}=\left(1+\frac{1}{\lambda}\right)\frac{\mu_{hnf}}{\rho_{hnf}}\frac{\partial^2 u}{\partial y^2}-\frac{\sigma_{hnf}}{\rho_{hnf}}B_0^2u-\frac{\mu_{hnf}}{\rho_{hnf}K*}u, \tag{6}$$

$$u\frac{\partial T}{\partial x}+v\frac{\partial T}{\partial y}=\frac{\kappa_{hnf}}{(\rho Cp)_{hnf}}\frac{\partial^2 T}{\partial y^2}-\frac{1}{(\rho Cp)_{hnf}}\frac{\partial q_r}{\partial y}+\frac{Q_0(T-T_\infty)}{(\rho Cp)_{hnf}}+\frac{\mu_{hnf}}{(\rho Cp)_{hnf}}\left(1+\frac{1}{\lambda}\right)\left(\frac{\partial u}{\partial y}\right)^2 +\frac{\sigma_{hnf}}{(\rho Cp)_{hnf}}(uB_0)^2, \tag{7}$$

$$u\frac{\partial C}{\partial x}+v\frac{\partial C}{\partial y}=D_b\frac{\partial^2 C}{\partial y^2}-Cr^*(C-C_\infty). \tag{8}$$

2.3. Boundary conditions for the fluid flow [1, 15, 26]

$$u=d_1\ x+L_1\frac{\partial u}{\partial y},\quad v=-\sqrt{a\nu_f}\ S,\quad T=T_w(x)=T_\infty+b\left(\frac{x}{l}\right)^n,\quad C=C_w=C_w+\left(\frac{x}{l}\right)^n C_\infty, \\ y=0.u=0,\quad v=0,\quad T\to T_\infty,\quad C\to C_\infty,\ \text{as}\ y\to\infty. \tag{9}$$

Rosseland approximation solved in terms of [1, 21].

$$q_r=-\frac{4\sigma^*T_\infty^3}{3k*}\frac{\partial T^4}{\partial y}, \tag{10}$$

$\Rightarrow \frac{\partial q_r}{\partial y}=-\frac{16\sigma*T_\infty^3}{3k*}\frac{\partial^2 T}{\partial y^2}$, where $T^4=(4T-3T_\infty)T_\infty^3$.

2.4. Similarity variables [1, 15, 26]

$$u=ax\ f'(\eta),\quad v=-f(\eta)\sqrt{a\nu_f},\quad \varphi=\frac{C-C_\infty}{C_w-C_\infty}, \\ T(\eta)=T_\infty+\Delta T\theta(\eta),\quad \eta=y\sqrt{\frac{a}{\nu_f}},\quad \Delta T=T_w-T_\infty. \tag{11}$$

Incorporating Equation (10) to Equation (7) to get

$$u\frac{\partial T}{\partial x}+v\frac{\partial T}{\partial y}=\left(\frac{\kappa_{hnf}}{(\rho Cp)_{hnf}}+\frac{1}{(\rho Cp)_{hnf}}\frac{16\sigma^*T_\infty^3}{3k^*}\right)\frac{\partial^2 T}{\partial y^2}+\frac{Q_0(T-T_\infty)}{(\rho Cp)_{hnf}}+\frac{\mu_{hnf}}{(\rho Cp)_{hnf}}\left(1+\frac{1}{\lambda}\right)\left(\frac{\partial u}{\partial y}\right)^2 +\frac{\sigma_{hnf}}{(\rho Cp)_{hnf}}(uB_0)^2, \tag{12}$$

n is the variable heat flux index, and by taking $n=2$ and nondimensional PDEs obtained as

$$\left(1+\frac{1}{\lambda}\right)A_1\ \frac{d^3f}{d\ \eta^3}+A_2f(\eta)\frac{d^2f}{d\ \eta^2}-A_2\left(\frac{d\ f}{d\ \eta}\right)^2-A_3\ M\frac{d\ f}{d\ \eta}\ -A_1\ Da^{-1}\frac{d\ f}{d\ \eta}=0, \tag{13}$$

$$\chi_1 \frac{d^2\theta}{d\eta^2} + A_5\left(f(\eta)\frac{d\theta}{d\eta} - 2\frac{d\,f}{d\eta}\theta(\eta)\right) + Ni\theta(\eta) + Ec\left[A_1\left(1+\frac{1}{\lambda}\right)\left(\frac{d^2\,f}{d\eta^2}\right)^2 + A_3\ M\left(\frac{d\,f}{d\eta}\right)^2\right] = 0, \tag{14}$$

$$\varphi_{\eta\eta}(\eta) + Sc\ f(\eta)\varphi_\eta(\eta) - Sc\left(2f_\eta(\eta) + Kc^*\right)\varphi(\eta) = 0. \tag{15}$$

where $A_1 = \frac{\mu_{hnf}}{\mu_f}, A_2 = \frac{\rho_{hnf}}{\rho_f}, A_3 = \frac{\sigma_{hnf}}{\sigma_f}$, $A_4 = \frac{\kappa_{hnf}}{\kappa_f}, A_5 = \frac{(\rho Cp)_{hnf}}{(\rho Cp)_f}$ are constants $M = \frac{\sigma_f B_0^2}{a\rho_f}$ is a magnetic parameter, $Nr = \frac{16\sigma * T_\infty^3}{3\kappa_f k*}$ is the thermal radiation, $Ni = \frac{Q_0}{a(\rho Cp)_f}$ is heat source/sink, $\Pr\left(=\frac{\mu_f(Cp)_f}{\kappa_f}\right)$ is a Prandtl number, $\chi_1 = \frac{(A_4+Nr)}{\Pr}$. $Da^{-1} = \frac{\nu_f}{K*a}$ is Porosity parameter, $Kc* = \frac{Cr*}{a}$ is the chemical reaction parameter, $Sc = \frac{\nu_f}{D_b}$ represents Schmidt number.

2.5. Modified boundary conditions [1, 15, 26]

$$\begin{gathered} f(0) = S, \quad f'(0) = d + Lf''(0), \quad \theta(0) = 1, \quad \varphi(0) = 1, \quad \text{at } \eta = 0, \\ f'(\infty) = 0, \quad \theta(\infty) = 0, \quad \varphi(\infty) = 0, \quad \text{as } \eta \to \infty. \end{gathered} \tag{16}$$

here $S\left(=-\frac{v_w}{\sqrt{av_f}}\right)$ denotes the mass transpiration, $d = \frac{d_1}{a}$ is a stretching/shrinking parameter, $L = L_1\sqrt{\frac{a}{\nu_f}}$ is a velocity slip parameter.

3. Analytic solution for momentum equation

By boundary condition Equation (11) we calculate the solution for Equation (13) as follows [see 34, 38, 39].

$$f(\eta) = S + d\frac{1-e^{-\beta\eta}}{\beta(1+L\beta)}. \tag{17}$$

By using the above equation, we solve Equation (13) and obtain the algebraic solution as follows:

$$\begin{gathered} \left(LA_1\left(1+\frac{1}{\lambda}\right)\right)\beta^3 - (A_3ML + A_2S + A_1Da^{-1}L)\beta - (A_2d + A_3M + A_1Da^{-1}) \\ + \left(A_1\left(1+\frac{1}{\lambda}\right) - A_2SL\right)\beta^2 = 0, \end{gathered} \tag{18}$$

the above equation is rewritten as

$$\xi_1\beta^3 + \xi_2\beta^2 + \xi_3\beta + \xi_4 = 0, \tag{19}$$

here

$$\begin{gathered} \xi_1 = A_1L\left(1+\frac{1}{\lambda}\right), \quad \xi_3 = -A_3ML - A_2S - A_1Da^{-1}L, \\ \xi_4 = -A_2d - A_3M - A_1Da^{-1}, \quad \xi_2 = A_1\left(1+\frac{1}{\lambda}\right) - A_2SL. \end{gathered} \tag{20}$$

All possible roots of the above Equation (18) are given as

$$\beta_1 = \frac{-\frac{\xi_2}{3\xi_1} - \left(2^{1/3}\left(-\xi_2^2 + 3\xi_1\xi_3\right)\right)}{3\xi_1\left(z + \sqrt{4\left(-\xi_2^2 + 3\xi_1\xi_3\right)^3 + (z)^2}\right)^{1/3}} + \frac{1}{3\quad 2^{1/3}\xi_1}\left(z + \sqrt{4\left(-\xi_2^2 + 3\xi_1\xi_3\right)^3 + (z)^2}\right)^{1/3},$$

$$\beta_2 = \frac{-\frac{\xi_2}{3\xi_1} + \left(\left(1 + i\sqrt{3}\right)\left(-\xi_2^2 + 3\xi_1\xi_3\right)\right)}{3\ \xi_1 2^{1/3}\left(z + \sqrt{4\left(-\xi_2^2 + 3\xi_1\xi_3\right)^3 + (z)^2}\right)^{1/3}}$$
$$-\frac{1}{6\xi_1 2^{1/3}}\left(1 + i\sqrt{3}\right)\left(z + \sqrt{4\left(-\xi_2^2 + 3\xi_1\xi_3\right)^3 + (z)^2}\right)^{1/3},$$

$$\beta_3 = \frac{-\frac{\xi_2}{3\xi_1} + \left(\left(1 + i\sqrt{3}\right)\left(-\xi_2^2 + 3\xi_1\xi_3\right)\right)}{3\ \xi_1 2^{1/3}\left(z + \sqrt{4\left(-\xi_2^2 + 3\xi_1\xi_3\right)^3 + (z)^2}\right)^{1/3}}$$
$$+\frac{1}{6\xi_1 2^{1/3}}\left(1 + i\sqrt{3}\right)\left(z + \sqrt{4\left(-\xi_2^2 + 3\xi_1\xi_3\right)^3 + (z)^2}\right)^{1/3} \tag{21}$$

here

$$z = \left(-2\xi_2^3 + 9\xi_1\xi_2\xi_3 - 27\xi_1^2\xi_4\right).$$

4. Exact solution of the temperature equation

We chose variable t to solve the Equation (14) as follows [see 34, 38, 39].

$$t = -e^{-\beta\eta}, \tag{22}$$

by using Equation (22) the energy equation is calculated as

$$t\frac{\partial^2\theta}{\partial t^2} + (1 - \xi_5 S - \xi_6(1 + t))\frac{\partial\theta}{\partial t} + \left(\xi_7 + \frac{Ni_1}{t}\right)\theta(\eta) = -Ec_1 t, \tag{23}$$

here

$$\xi_5 = -\frac{A_5}{\chi_1\beta}, \quad \xi_6 = \frac{A_5 d}{\chi_1\beta^2(1 + L\beta)}, \xi_7 = \frac{2A_5 d}{\chi_1\beta^2(1 + L\beta)}, \quad Ni_1 = \frac{Ni}{\chi_1\beta^2},$$

Modified boundary conditions are [38, 39].

$$\theta(t = -1) = 1, \quad \theta(t = 0) = 0, \tag{25}$$

eq. (23) and (25) solved as

$$\theta(t) = (1 - B_3)(-t)^{B_2}\frac{\text{Laguerre}[B_1, B_2, \xi_6 t]}{\text{Laguerre}[B_1, B_2, -\xi_6]} + B_3 t^2, \tag{26}$$

$L[a, b, z]$ are the generalized Laguerre polynomials, B_1, B_2, and B_3 are as follows:

$$B_1 = m_1 - \frac{\xi_7}{\xi_6}, \quad B_2 = 2m_1 + m_2, \ B_3 = \frac{Ec_1}{2 + 2m_2 + Ni_1},$$

The temperature solution is calculated as follows

$$\theta'(-1) = -\frac{(1-B_3)}{\text{Laguerre}[B_1, B_2, -\xi_6]}\left[\text{B}_2\text{Laguerre}[B_1, B_2, -\xi_6] + \xi_6 \text{Laguerre}_z[B_1, B_2, -\xi_6]\right] - 2B_3. \tag{28}$$

5. Analytic solution for concentration

Considered variable t to solve concentration equation as follows

$$t_1 = \frac{-Sc}{\beta^2} e^{-\beta\eta}, \tag{29}$$

by using Equation (15) concentration equation is calculated as

$$t_1 \frac{\partial^2 \varphi}{\partial {t_1}^2} + [1 - C_1 - \alpha t_1] \frac{\partial \varphi}{\partial t_1} + \left(2\alpha - \frac{Kc^* Sc}{\beta^2 t_1}\right) = 0, \tag{30}$$

corresponding boundary conditions are as follows:

$$\varphi\left(-\frac{Sc}{\beta^2}\right) = 1, \quad \varphi(0) = 0. \tag{31}$$

The Frobenius method is utilized to examine the φ, i.e.,

$$\varphi(t_1) = \sum_{r=0}^{\infty} a_r {t_1}^{r+k}, \tag{32}$$

derivatives Equation (32) followed as

$$\varphi_\eta(t_1) = \sum_{r=0}^{\infty} a_r (r+k) \xi^{r+k-1}, \tag{33}$$

$$\varphi_{\eta\eta}(t_1) = \sum_{r=0}^{\infty} a_r (r+k)(r+k-1) \xi^{r+k-2}. \tag{34}$$

Analytic solution of Equation (30) with B.C. (31) obtained as

$$\varphi(t1) = \left(\frac{-t_1}{Sc/\beta^2}\right)^{\frac{m_3}{2}} \frac{\text{Hypergeometric}[m_3 - 2; 2m_3 + 1 - C_1; \alpha t_1]}{\text{Hypergeometric}\left[m_3 - 2; 2m_3 + 1 - C_1; -\alpha \frac{Sc}{\beta^2}\right]}, \tag{35}$$

where

$$m_3 = C_1 + \sqrt{C_1^2 + 4ScKc*/\beta^2}, C_1 = \frac{ScS}{\beta} + \frac{Scd}{\beta^2(1+L\beta)}, \quad \alpha = \frac{d}{(1+L\beta)}.$$

6. Physical quantities or engineering quantities

$$C_f = \frac{2\tau_w}{\rho_{hnf} u_w^2}, \tag{36}$$

$\text{Re}_x = \frac{a\ x^2}{\nu_f}$ denotes the local Reynolds number.
wall shear stress $\tau_w = \mu_{hnf}\left(1 + \frac{1}{\lambda}\right)\left(\frac{\partial u}{\partial y}\right)_{y=0}$,
by using the above equation skin friction is calculated as follows

$$\frac{C_f\sqrt{\mathrm{Re}_x}}{2} = \left(1+\frac{1}{\lambda}\right)\frac{A_1}{A_2}f''(0).$$

Nusselt numbers are calculated as follows.

$$Nu = \frac{xq_w}{\kappa_f(T_w - T_\infty)}, \tag{37}$$

heat flux of the surface $q_w = -\left(\kappa_{hnf} + \frac{16\sigma * T_\infty^3}{3k*}\right)\left(\frac{\partial T}{\partial y}\right)_{y=0}$,

by using the above equation Nusselt number is calculated as follows

$$(\mathrm{Re}_x)^{-0.5}Nu = -(A_4 + Nr)\theta'(0).$$

Sherwood numbers are calculated as follows.

$$S_{hx} = \frac{xJ_w}{D_b(C_w - C_\infty)} \quad \text{where} \quad J_w = -D_b\frac{\partial C}{\partial y}\Big|_{y=0}, \tag{38}$$

J_w is known as mass flux from the sheet, by solving able equation we get

$$S_{hx}(\mathrm{Re}_x)^{-0.5} = -\varphi'(0). \tag{39}$$

7. Solution for entropy generation

The following mathematical formula represents the rate of dimensional entropy formation during radiative heat transfer in magnetic fields [22, 23].

$$Sg = \frac{\kappa_f}{T_\infty^2}\left[\frac{\kappa_{hnf}}{\kappa_f} + \frac{16\sigma^* T_\infty^3}{3k^*\kappa_f}\right]\left(\frac{\partial T}{\partial y}\right)^2 + \frac{\mu_{hnf}}{T_\infty}\left(1+\frac{1}{\lambda}\right)\left(\frac{\partial u}{\partial y}\right)^2 + \frac{\sigma_{hnf}}{T_\infty}(uB_0)^2 + \frac{\mu_{hnf}}{K^* T_\infty}(u)^2, \tag{40}$$

Table 1. Thermophysical properties of sodium alginate, aluminum oxide, and silicon dioxide [27–29].

Properties	*SA*	Al_2O_3	SiO_2
σ	2.6×10^{-4}	10^{-12}	1×10^{-18}
ρ	989	3970	2650
Cp	4175	765	730
κ	0.6376	40	1.5

Table 2. Thermophysical properties of hybrid nanofluid [27–29].

Dynamic viscosity	$\frac{\mu_{hnf}}{\mu_f} = \frac{1}{(1-\phi_1)^{2.5}(1-\phi_2)^{2.5}}$.
Density	$\frac{\rho_{hnf}}{\rho_f} = (1-\phi_2)(1-\phi_1+\phi_1\left(\frac{\rho_{s_1}}{\rho_f}\right)) + \phi_2\left(\frac{\rho_{s_2}}{\rho_f}\right)$.
Electrical conductivities	$\frac{\sigma_{hnf}}{\sigma_f} = \frac{\sigma_{s_2} + 2\sigma_{bf} + 2\phi_2(\sigma_{s_2} - \sigma_f)}{\sigma_{s_2} + 2\sigma_{bf} - \phi_2(\sigma_{s_2} - \sigma_f)}$ where $\frac{\sigma_{bf}}{\sigma_f} = \frac{\sigma_{s_1} + 2\sigma_f + 2\phi_1(\sigma_{s_1} - \sigma_f)}{\sigma_{s_1} + 2\sigma_f - \phi_1(\sigma_{s_1} - \sigma_f)}$.
Heat capacitance	$\frac{(\rho Cp)_{hnf}}{(\rho Cp)_f} = (1-\phi_2)(1-\phi_1+\phi_1(\frac{(\rho Cp)_{s_1}}{(\rho Cp)_f})) + \phi_2(\frac{(\rho Cp)_{s_2}}{(\rho Cp)_f})$
Thermal conductivity	$\frac{\kappa_{hnf}}{\kappa_f} = \frac{\kappa_{s_2} + 2\kappa_{bf} + 2\phi_2(\kappa_{s_2} - \kappa_f)}{\kappa_{s_2} + 2\kappa_{bf} - \phi_2(\kappa_{s_2} - \kappa_f)}$ where $\frac{\kappa_{bf}}{\kappa_f} = \frac{\kappa_{s_1} + 2\kappa_f + 2\phi_1(\kappa_{s_1} - \kappa_f)}{\kappa_{s_1} + 2\kappa_f - \phi_1(\kappa_{s_1} - \kappa_f)}$.

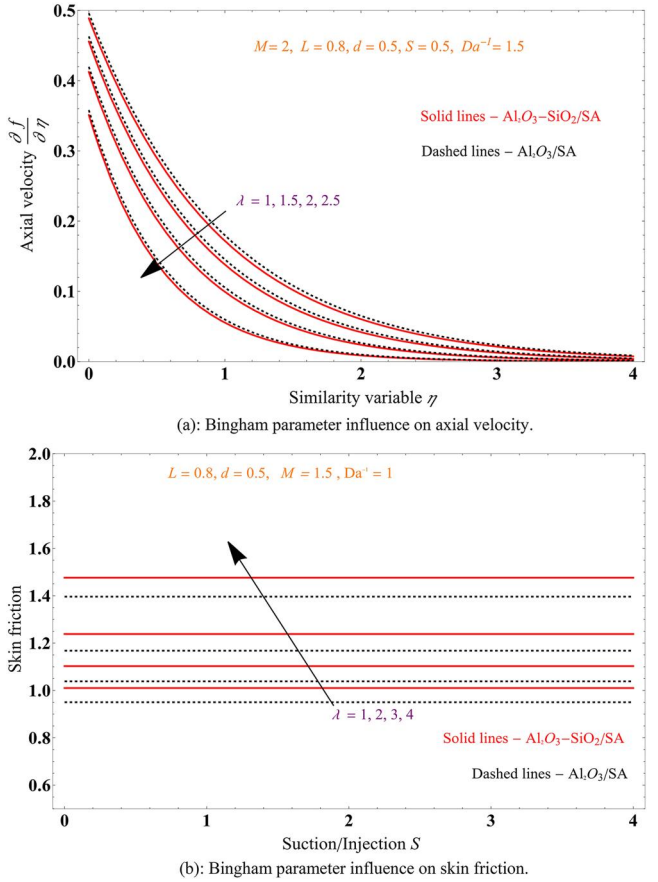


Figure 2. (a) Bingham parameter influence on axial velocity. (b) Bingham parameter influence on skin friction.

$$\begin{aligned}\text{Heat transfer} &\Rightarrow \frac{\kappa_f}{T_\infty^2}\left[\frac{\kappa_{hnf}}{\kappa_f}+\frac{16\sigma^* T_\infty^3}{3k^*\kappa_f}\right]\left(\frac{\partial T}{\partial y}\right)^2,\\ \text{Fluid friction} &\Rightarrow \frac{\mu_{hnf}}{T_\infty}\left(1+\frac{1}{\lambda}\right)\left(\frac{\partial u}{\partial y}\right)^2+\frac{\mu_{hnf}}{K^* T_\infty}u^2,\\ \text{Joule heating} &\Rightarrow \frac{\sigma_{hnf}}{T_\infty}(uB_0)^2,\end{aligned} \tag{41}$$

solution of entropy production rate obtained as

$$Ng=(A_4+Nr)\delta(\theta')^2+Br\left[A_1\left(1+\frac{1}{\lambda}\right)(f'')^2+A_3M(f')^2+A_1Da^{-1}(f')^2\right], \tag{42}$$

where $Br = Ec \times \Pr$, and $\delta = \frac{T_w - T_\infty}{T_\infty}$.

In the next section, we study the graphical analysis of several physical parameters included in our study.

8. Results and discussion

The present article determines the effects of engineering quantities on chemically reactive magnetic sodium alginate fluid flow with heat and mass transfer with entropy generation analysis, nonlinear governing equations scrutinized to ODEs by using similarity terms, heat generation,

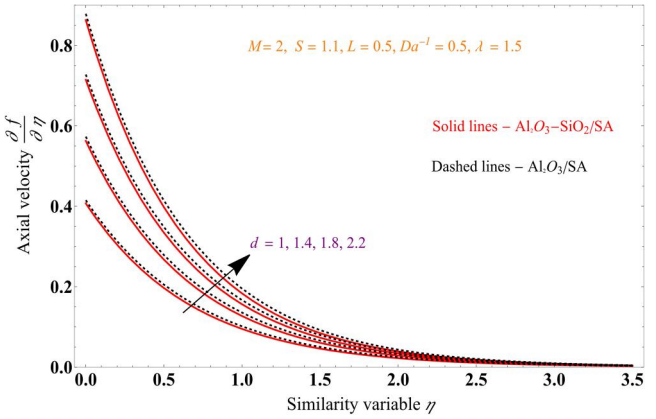
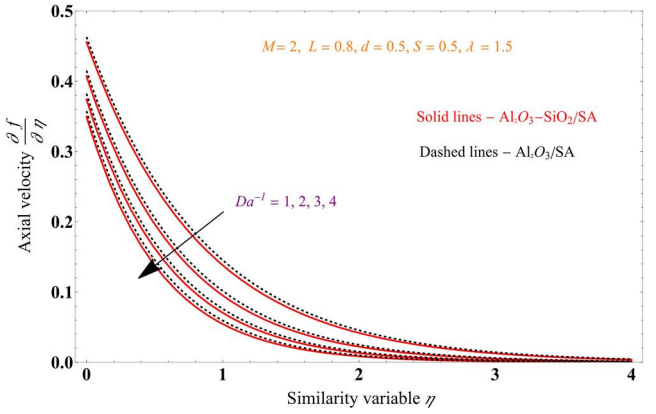
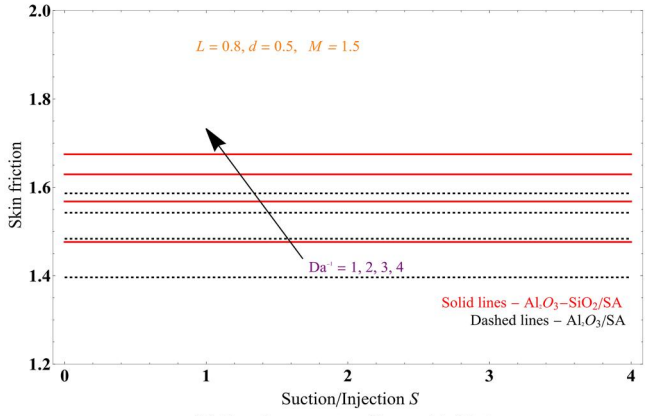


Figure 3. Stretching parameter influence on axial velocity.



(a): Porosity parameter influence on axial velocity.



(b): Porosity parameter effect on skin friction.

Figure 4. (a) Porosity parameter influence on axial velocity. (b) Porosity parameter effect on skin friction.

and solar radiation considered temperature equations, and formulated by using the Luggerel method. Thermophysical properties are stated in Tables 1 and 2, and several physical terms are analyzed through plots as follows:

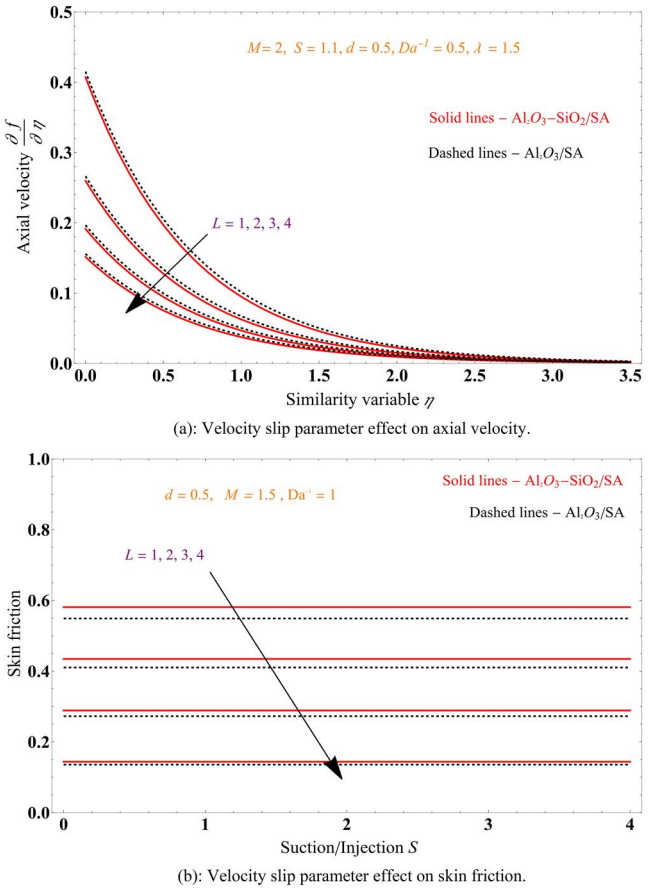
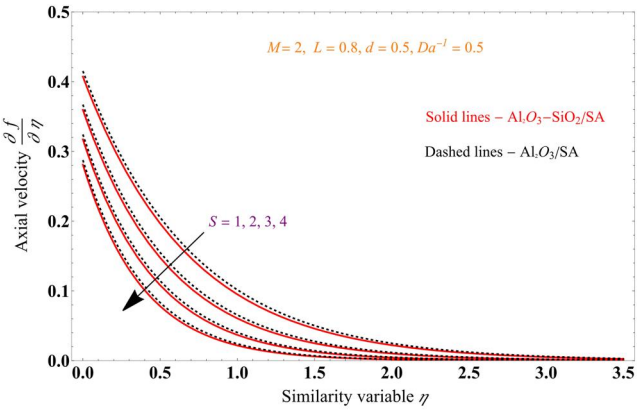


Figure 5. (a) Velocity slip parameter effect on axial velocity. (b) Velocity slip parameter effect on skin friction.

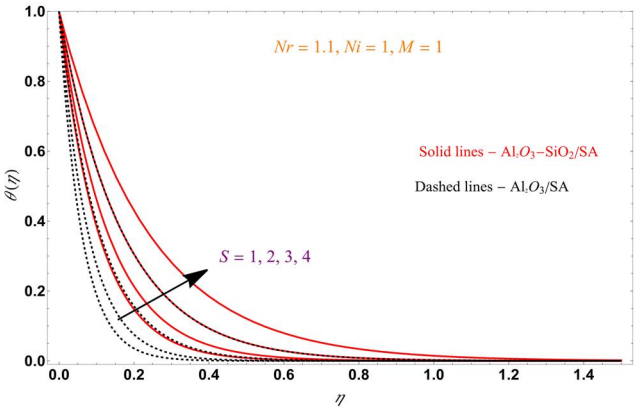
Figure 2(a) and (b) represent the axial momentum and skin friction graphs for various choices of the Bingham parameter. For graphs taken for both unary and binary nanofluid flow, increasing the Bingham parameter decreases the momentum and increases the skin friction. Physically, this is because the higher yield stress of the Bingham plastic fluid requires more stress to initiate flow, resulting in lower velocities and raising skin friction. Understanding the Bingham term is essential for various real-world applications, such as in the petroleum industry for drilling mud flow and in civil engineering for concrete slurry transport.

Figure 3 portrays the axial momentum plots for different numbers of stretching parameters, graphs taken for both unary and binary nanofluid flow; raising the stretching term improves the flow of the fluid. Physically, the velocity boundary layer thickness upsurges as the stretching term increases due to the opposition to fluid flow by greater viscosity.

Figure 4(a) and (b) represent the axial momentum and skin friction graphs for various choices of porosity parameter. For graphs taken for both unary and binary nanofluid flow, improving the porosity parameter reduces the velocity and increases the skin friction. Physically, higher fluid velocities and lower permeabilities lead to greater dispersion of tracers in porous media due to the velocity differences caused by the porous structure. An upsurge in the porosity (which corresponds to a decrease in permeability) causes greater retardation to the fluid momentum, resulting in a thinner velocity boundary layer. This is because of resistance to fluid flow caused by the permeable surface, which raises the skin friction. Porous media is essential for optimizing processes



(a): Mass transpiration parameter impact on velocity.



(b): Mass transpiration impact on temperature.

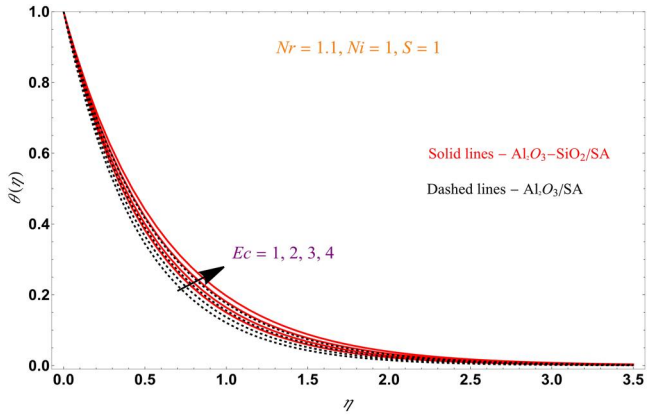
Figure 6. (a) Mass transpiration parameter impact on velocity. (b) Mass transpiration impact on temperature.

like groundwater remediation and oil recovery, ranging from water filtration systems to the design of efficient thermal insulation materials.

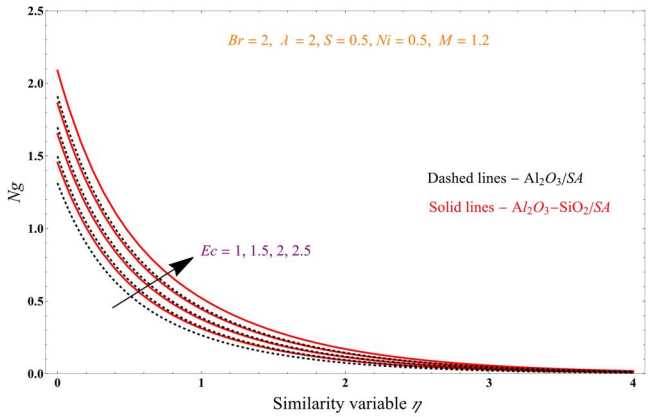
Figure 5(a) and (b) represent the axial momentum and skin friction graphs for different choices of velocity slip. For graphs taken for both unary and binary nanofluid flow, improving the velocity slip term decreases the momentum and the skin friction. Physically, the skin friction coefficient reduces with an upsurge in the velocity slip term. This is because the slip at the wall reduces the shear stress and hence the skin friction. Velocity slip can contribute to the optimization of airflow over aircraft surfaces, potentially enhancing fuel efficiency and reducing drag.

Figure 6(a) and (b) represent the axial momentum and temperature graphs for various numbers of mass transpiration parameters. For graphs taken for both unary and binary nanofluid flow, improving the mass transpiration term slowdowns the momentum and upsurges the temperature. Physically, suction opposes the flow of the fluid near the heated surface, reducing the momentum boundary layer thickness. This is because the mass transpiration brings the ambient fluid closer to the surface, enhancing heat transfer. The thinner velocity boundary layer caused by mass transpiration also implies a thicker thermal boundary layer. This reduces the amount of fluid available to conduct heat from the solid surface, raising thermal conduction.

Figure 7(a) and (b) represent the energy and entropy generation graphs for different values of the *Ec* parameter. For graphs taken for both unary and binary nanofluid flow, enhancing the *Ec* parameter raises the energy and entropy generation, the *Ec* is a non-dimension term that portrays the ratio of kinetic energy to enthalpy, and it quantifies the impact of viscous dissipation on heat



(a): Eckert number parameter effect on temperature.



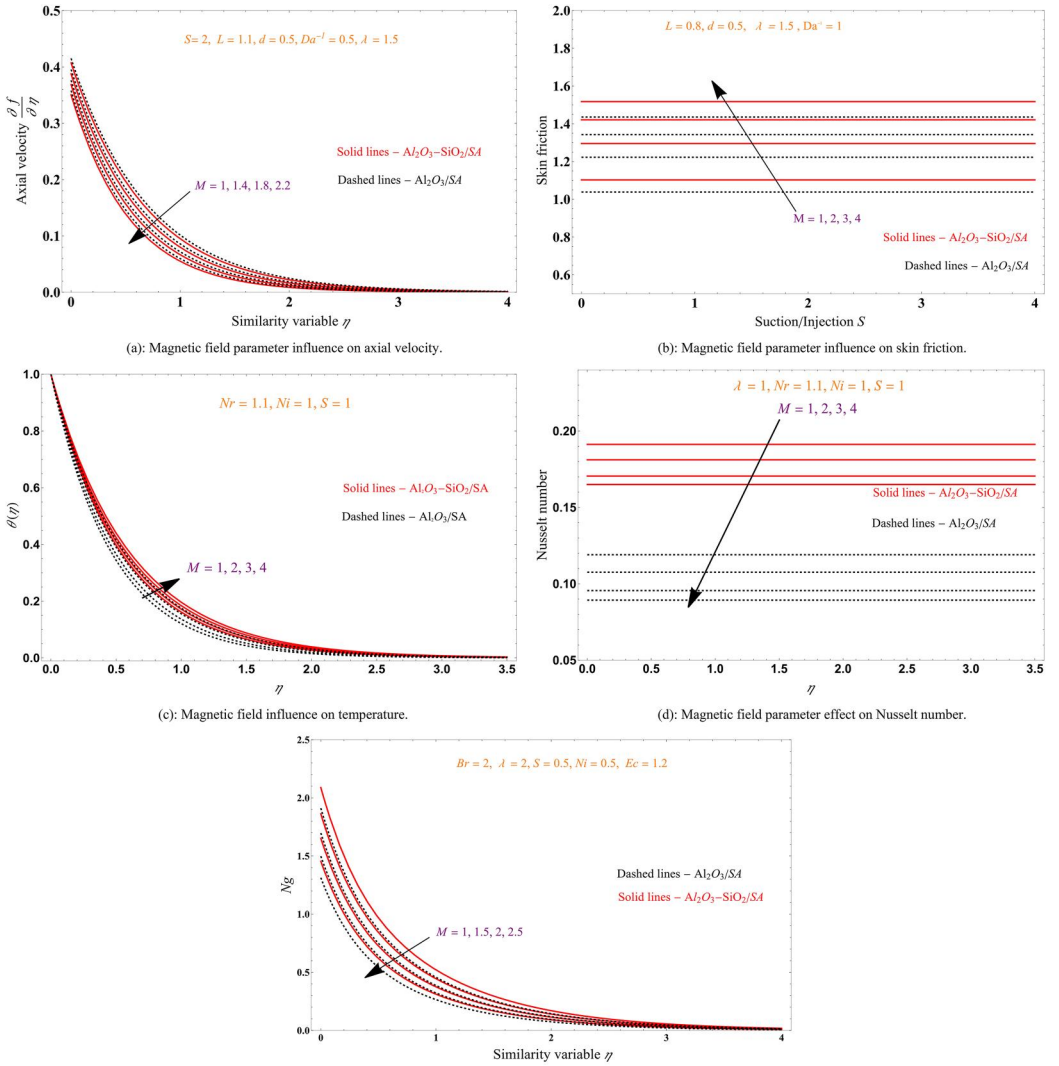
(b): Eckert number parameter effect on entropy generation.

Figure 7. (a) Eckert number parameter effect on temperature. (b) Eckert number parameter effect on entropy generation.

transfer. Increasing the *Ec* significantly enhance the entropy generation as it enhances the dissipative heat transfer effects.

Figures 8(a) and (b) represent the axial velocity and skin friction graphs for different numbers of magnetic field term. For graphs taken for both unary and binary nanofluid flow, raising the magnetic field parameter enhances the skin friction and reduces the velocity. Figures 8 (c), (d), and (e) represent the temperature, Nusselt number, and entropy generation graphs for various quantities of magnetic field term; increasing the parameter *M* upsurges the temperature and decreases the Nusselt number and entropy generation. Physically, a stronger magnetic field tends to a higher energy profile in the fluid flow. This is attributed to the Lorentz force restricting the fluid flow, which allows for more heat transfer; the average Nusselt number decreases with increasing magnetic field, especially at higher Rayleigh numbers where convection is dominant. The magnetic field damps the flow field and weakens convection currents, leading to reduced Nusselt numbers.

Plots 9(a) and (b) represent the energy and entropy generation graphs for various values of thermal radiation parameters; increasing the *Nr* term increases the temperature and entropy generation. Figure 9(c) portrays the Nusselt number graph for different values of the radiation parameter; higher choices of the radiation parameter led to a major enhancement of the Nusselt number, reflecting the strong impact of radiation on the heat transfer process. Additionally, thermal radiation upsurges the entropy generation closer to the heated surface. This is because the increased heat transfer due to radiation leads to higher irreversibility's near the boundary. The



(a): Magnetic field parameter influence on axial velocity.

(b): Magnetic field parameter influence on skin friction.

(c): Magnetic field influence on temperature.

(d): Magnetic field parameter effect on Nusselt number.

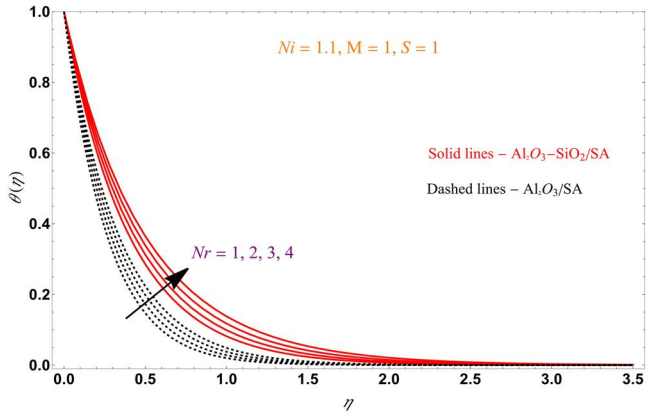
(e): Magnetic field parameter effect on entropy generation.

Figure 8. (a) Magnetic field parameter influence on axial velocity. (b) Magnetic field parameter influence on skin friction. (c) Magnetic field influence on temperature. (d) Magnetic field parameter effect on Nusselt number. (e) Magnetic field parameter effect on entropy generation.

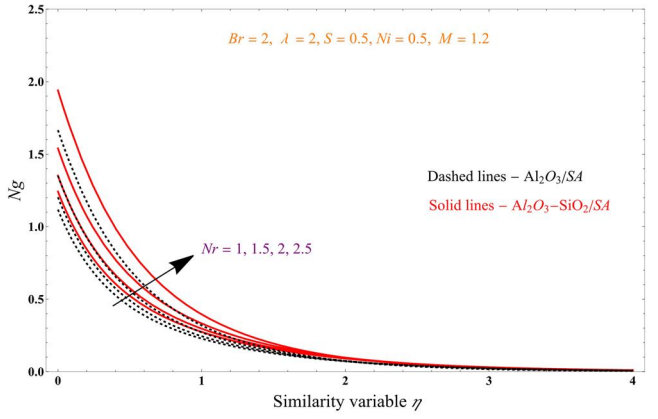
management of thermal radiation can affect the boundary layer of fluids, impacting vehicle performance and safety. In energy production, such as solar power technology.

Figure 10(a) and (b) represent the entropy generation and temperature plots for different numbers of the heat source term. For graphs taken for both unary and binary nanofluid flow, improving the heat generation term raises the energy and entropy generation. Physically, the presence of a heat generation within the fluid enhances the temperature distribution, leading to higher temperature gradients near the heat generation. This results in a reduce in the local Nusselt number, especially near the corners of the heat source. The heat source parameters are vital for maximizing energy output while minimizing environmental impact.

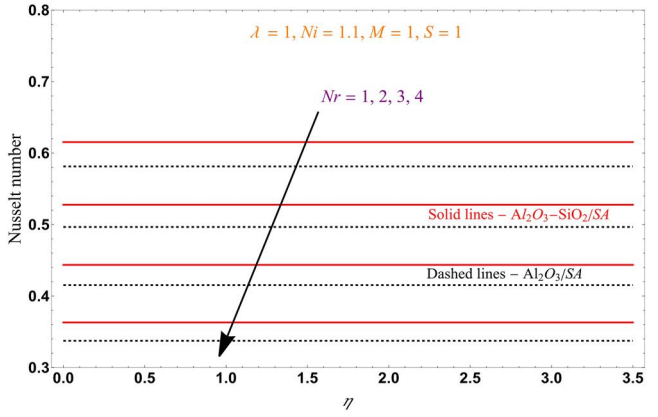
Figure 11(a) and (b) portray the concentration and Sherwood graphs for different values of the Schmidt parameter, graphs taken for both unary and binary nanofluid flow, improving the Schmidt parameter slowdowns the concentration and raises the Sherwood number. Physically, the



(a): Radiation parameter effect on temperature.



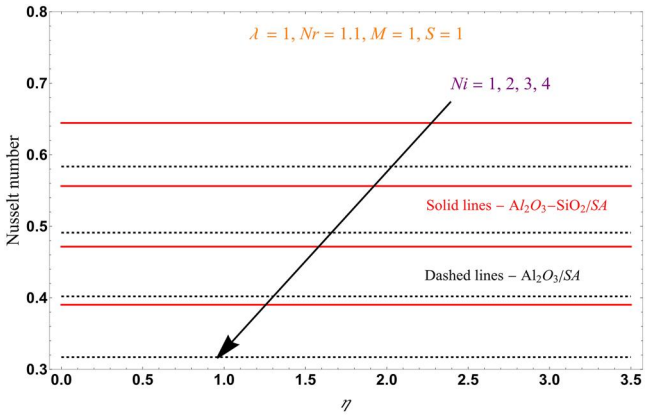
(b): Radiation parameter effect on entropy generation.



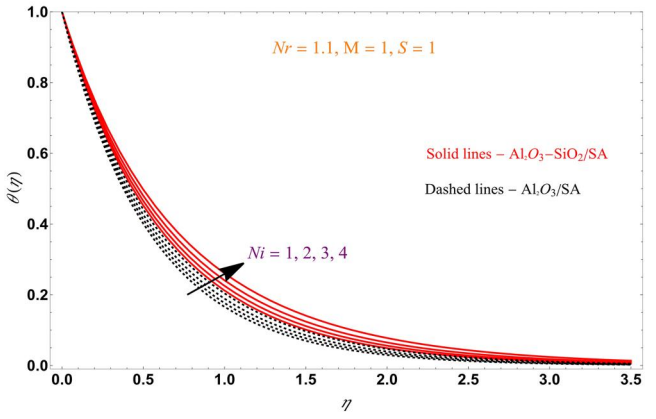
(c): Radiation parameter effect on Nusselt number.

Figure 9. (a) Radiation parameter effect on temperature. (b) Radiation parameter effect on entropy generation. (c) Radiation parameter effect on Nusselt number.

Sc is a non-dimensional quantity that denotes the ratio of the kinematic viscosity to the mass diffusivity. As the Schmidt number increases, the mass transfer rate increases, and consequently the concentration profiles decrease. As the Schmidt number increases, the mass diffusion rate decreases relative to the momentum diffusion rate, leading to a higher Sherwood number and higher mass transfer rate.



(a): Heat source term effect on Nusselt number.



(b): Heat source term influence on temperature.

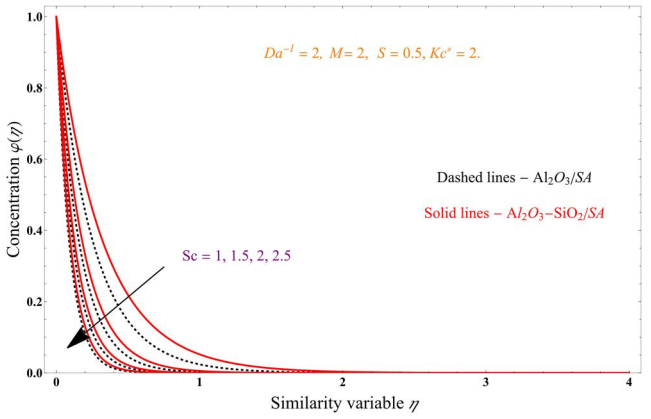
Figure 10. (a) Heat source term effect on Nusselt number. (b) Heat source term influence on temperature.

Figure 12(a) and (b) portray the concentration and Sherwood graphs for various choices of the chemical reaction parameter. For graphs taken for both unary and binary nanofluid flow, enhancing the Kc* parameter decreases the concentration and raises the Sherwood number. Physically, this is because higher mass transfer means more reactant particles in the same volume, leading to a greater number of collisions between the reactants, a higher concentration results in a faster reaction rate. A higher chemical reaction rate leads to a greater mass transfer rate between the fluid and the sheet, giving a higher Sherwood number. The Sherwood number quantifies this mass transfer rate.

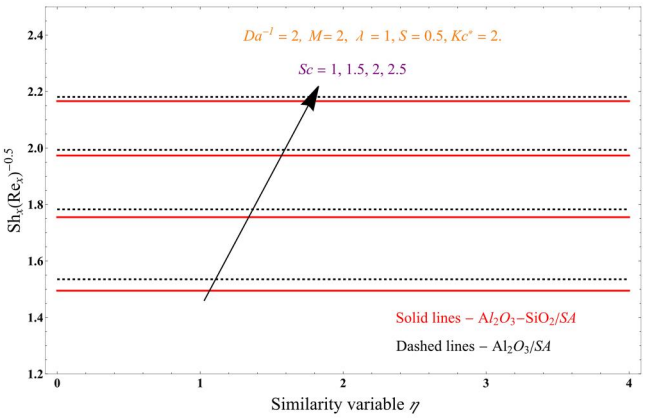
Figure 13(a-f): Stream lime graphs for different choices of the Bingham parameter, porosity parameter, and magnetic field. Figure 13(a-f) portrays the stream lime graphs for various choices of the Bingham parameter, porosity parameter, and magnetic field, graphs taken for both unary and binary nanofluid flow. Streamline graphs are a fascinating way to visualize vector fields and fluid flow. They represent the motion of particles in a fluid, showing paths that are tangent to the velocity field at every point. Streamline graphs can help predict weather patterns, design more efficient machinery, and even illustrate abstract concepts in physics and mathematics.

9. Concluding remarks

The current article aims to determine the effects of engineering quantities on chemically reactive magnetic Sodium Alginate fluid flow with heat and mass transfer with entropy generation



(a): Schmidt parameter effect on concentration.

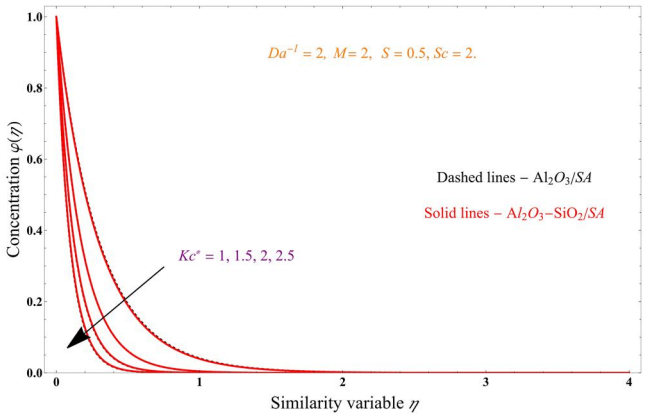


(b): Schmidt parameter effect on Sherwood number.

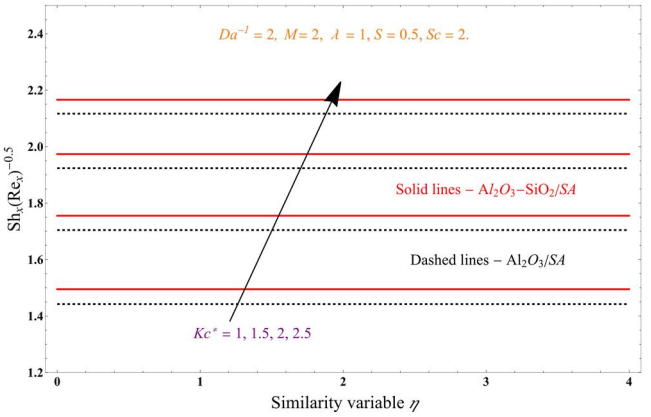
Figure 11. (a) Schmidt parameter effect on concentration. (b) Schmidt parameter effect on Sherwood number.

analysis, nonlinear governing equations scrutinized to ODEs by using similarity transformations, heat generation/absorption, and radiation effects considered in temperature equations, and formulated by using the Luggerel method. Table 3 represents the comparison table of the current study with other works; Table 4 represents the effects of different physical terms on fluid flow. The analysis shows that there are major variations in the flow and thermal characteristics due to the changes in the parameters that govern the system. An enhance in the magnetic parameter raises the temperature by about 21%, which is something that can be attributed to the strong Lorentz force damping and the Joule heating effects, respectively. The heat transfer rate (Nusselt number) increases by about 22% when the heat source changes from 1 to 4 and by around 28% with a similar increase in the thermal radiation parameter, thus the transport of heat is strongly influenced. The temperature and entropy generation proceed to be greatly affected by the Eckert number, mainly due to viscous dissipation. Besides that, the intensification of the chemical reaction as well as the Schmidt number, they both lead to the reduction in concentration and increase in the Sherwood number, which thus reflects the increase in the mass transfer rates. The findings of the current analysis are obtained as below:

- Enhancing the Bingham term decreases the velocity and increases the skin friction due to higher yield stress which is used in cooling systems for electrical devices.
- Increasing the velocity slip parameter upsurges the momentum and decreases the skin friction due to drag force.



(a): Chemical reaction effect on concentration.



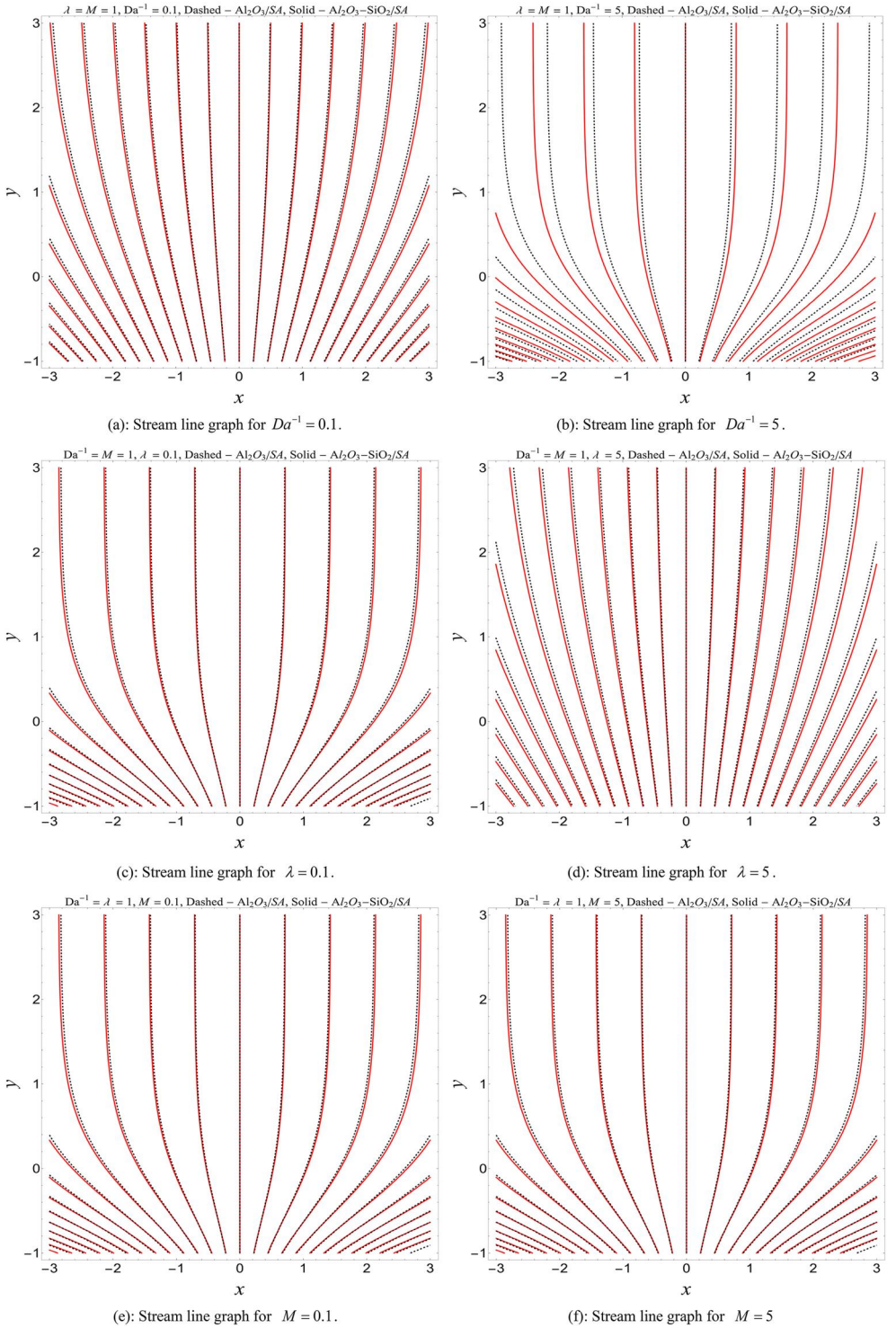
(b): Chemical reaction effect on Sherwood number.

Figure 12. (a) Chemical reaction effect on concentration. (b) Chemical reaction effect on Sherwood number.

- Increasing the thermal radiation upsurges the entropy generation and temperature and decreases the Nusselt number.
- Raising the magnetic term increases the temperature and entropy generation, the magnetic field is utilized to influence the flow of blood, which is an electrically conducting fluid, for targeted drug delivery systems.
- Chemical reaction and Schmidt number raise the Sherwood number and decrease the temperature.
- Increasing the porosity parameter decreases the velocity of the fluid flow and increases the skin friction due to resistance created by the porous structure.
- Enhancing the Eckert number increases the temperature as well as entropy generation.

The limiting cases of the current analysis:

- $\lim_{\substack{Da^{-1} \to 0 \\ \lambda \to \infty \\ S \to 0 \\ Ni,\ Nr \to 0}} \{\text{our results}\} \to \{\text{results of Wang [37]}\}.$
- $\lim_{\substack{Qo \to 0 \\ \phi,\ \varphi \to 0 \\ Da^{-1} \to 0}} \{\text{our results}\} \to \{\text{results of Usafzai [38]}\}.$



(a): Stream line graph for $Da^{-1} = 0.1$.

(b): Stream line graph for $Da^{-1} = 5$.

(c): Stream line graph for $\lambda = 0.1$.

(d): Stream line graph for $\lambda = 5$.

(e): Stream line graph for $M = 0.1$.

(f): Stream line graph for $M = 5$

Figure 13. (a) Stream line graph for $Da^{-1} = 0.1$. (b) Stream line graph for $Da^{-1} = 5$. (c) Stream line graph for $\lambda = 0.1$. (d) Stream line graph for $\lambda = 5$. (e) Stream line graph for $M = 0.1$. (f) Stream line graph for $M = 5$.

Table 3. Comparison table of the current study with other works.

Related Works by Other Authors	Fluids	Value of Momentum solution
Crane 1970 [40]	Newtonian	$\beta = 1$
Pavlov 1974 [41]	Newtonian	$\beta = \sqrt{1+M}$
U. Khan [39]	Non-Newtonian	$f(\eta) = f_w + \frac{\lambda}{\beta}(1 - \exp[-\beta\eta])$, $\beta = \frac{3f_w\left(\frac{\rho_{hnf}}{\rho_f}\right) \pm \sqrt{9f_w^2\left(\frac{\rho_{hnf}}{\rho_f}\right)^2 + 4\left(\frac{\mu_{hnf}}{\mu_f}\right)3\lambda\left(\frac{\rho_{hnf}}{\rho_f}\right) + \left(\frac{\sigma_{hnf}}{\sigma_f}\right)M}}{2\left(\frac{\mu_{hnf}}{\mu_f}\right)}$,
Present work	Non-Newtonian	$f(\eta) = S + d\frac{1-e^{-\beta\eta}}{\beta(1+L\beta)}$. $\left(LA_1\left(1+\frac{1}{\lambda}\right)\right)\beta^3 + \left(A_1\left(1+\frac{1}{\lambda}\right) - A_2SL\right)\beta^2 - (A_3ML + A_2S + A_1Da^{-1}L)\beta - (A_2d + A_3M + A_1Da^{-1}) = 0$,

Table 4. Effects of several physical terms on fluid flow.

Parameters	Velocity profile	Temperature	Entropy generation	Skin friction	Nusselt number	concentration
Bingham parameter	decreases	–	–	increases	–	–
Stretching parameter	increases	–	–		–	–
Porosity parameter	decreases	–	–	increases	–	–
Velocity slip	decreases	–	–	decreases	–	–
Mass suction	decreases	increases	–	–	–	–
Eckert number	–	increases	–	–	increases	–
Magnetic field	decreases	increases	decreases	increases	decreases	–
Thermal radiation	–	increases	increases	–	decreases	–
Heat source	–	increases	–	–	decreases	–
Schmidt number	–	–	–	–	–	decreases
Chemical reaction	–	–	–	–	–	decreases

- $\lim_{\substack{\phi,\ \varphi \to 0 \\ Ni,\ Nr \to 0 \\ Da^{-1} \to 0}}$ {our results}→{results of U. Khan [39]}.
- $\lim_{\substack{\beta \to 0 \\ \gamma \to 0 \\ S \to 0}}$ {our results}→{results of Crane [40]}.

The present analysis can be extended by utilizing various physical effects such as buoyancy forces, activation energy, viscoelastic behavior, or non-Newtonian fluid characteristics can be integrated into the analysis. These enhancements can be explored within a range of geometric configurations, including but not limited to stretching or shrinking sheets, rotating disks, cylindrical surfaces, wedges, converging or diverging channels, Riga plates, and microchannels.

9.1. Limitations of the present study

The present study relies on the following main simplifying assumptions: the flow is steady, laminar, two-dimensional, and incompressible. In addition, the porous medium is assumed to be homogeneous and isotropic, and the nanoparticles are considered to be uniformly dispersed without any agglomeration or sedimentation, etc. The magnetic field is assumed uniform, and thermal radiation is represented through the Rosseland approximation. However, these simplifications may reduce the extent to which the findings can be directly applied to complex real-world systems.

Ethical approval

Not applicable.

Disclosure statement

No potential conflict of interest was reported by the author(s).

Funding

No fundings available for this work.

Data availability statement

The data that support the findings are available from corresponding author upon reasonable request.

References

[1] S. M. Sachhin, *et al.*, "Chemically reactive micropolar hybrid nanofluid flow over a porous surface in the presence of an inclined magnetic field and radiation with entropy generation," *Physics*, vol. 6, no. 4, pp. 1315–1344, 2024. DOI: 10.3390/physics6040082.

[2] M. Ajithkumar, P. Lakshminarayana and K. Vajravelu, "Diffusion effects on mixed convective peristaltic flow of a bi-viscous Bingham nanofluid through a porous medium with convective boundary conditions," *Physic. Fluids*, vol. 35, no. 3, pp. 032008, 2023. DOI: 10.1063/5.0142003.

[3] F. Sultan, N. A. Khan and M. I. Afridi, "Investigation of biological mechanisms during flow of nano-Bingham–Papanastasiou fluid through a diseased curved artery," Proceedings of the Institution of Mechanical Engineers, Part N: Journal of Nanomaterials, Nanoengineering and Nanosystems 234(3–4), pp. 69–81., 2020. DOI: 10.1177/2397791420911265.

[4] R. C, *et al.*, "Magnetohydrodynamic peristaltic flow of Bingham fluid in a channel: an application to blood flow," *JMES*, vol. 15, no. 2, pp. 8082–8094, 2021. DOI: 10.15282/jmes.15.2.2021.12.0637.

[5] M. Basavarajappa, S. Myson and K. Vajravelu, "Study of multilayer flow of a bi-viscous Bingham fluid sandwiched between hybrid nanofluid in a vertical slab with nonlinear Boussinesq approximation," *Physics of Fluids*, vol. 34, no. 12, pp. 122006, 2022. DOI: 10.1063/5.0123131.

[6] N. T. Eldabe, G. M. Moatimid and A. Sayed, "The effects of the pressure work and Hall currents in the MHD peristaltic flow of Bingham–Papanastasiou nanofluid through porous media," *Pramana - J Phys*, vol. 95, no. 2, pp. 76, 2021. DOI: 10.1007/s12043-021-02091-3.

[7] S. A. A. Shah, N. A. Ahammad, E. M. T. E. Din, F. Gamaoun, A. U. Awan and B. Ali, "Bio-convection effects on Prandtl hybrid nanofluid flow with chemical reaction and motile microorganism over a stretching sheet," *Nanomaterials*, vol. 12, no. 13, pp. 2174, 2022. DOI: 10.3390/nano12132174.

[8] N. Joshi, H. Upreti, A. K. Pandey and M. Kumar, "Heat and mass transfer assessment of magnetic hybrid nanofluid flow via bidirectional porous surface with volumetric heat generation," *Int. J. Appl. Comput. Math*, vol. 7, no. 3, pp. 64, 2021. DOI: 10.1007/s40819-021-00999-3.

[9] N. C. Roy and I. Pop, "Heat and mass transfer of a hybrid nanofluid flow with binary chemical reaction over a permeable shrinking surface," *Chinese Journal of Physics*, vol. 76, pp. 283–298, 2022. DOI: 10.1016/j.cjph.2021.10.041.

[10] S. Ahmed, Z.-M. Chen and M. Ishaq, "Multiple solutions in magnetohydrodynamic stagnation flow of hybrid nanofluid past a sheet with mathematical chemical reactions model and stability analysis," *Physics of Fluids*, vol. 35, no. 7, pp. 072002, 2023. DOI: 10.1063/5.0157429.

[11] Y.-X. Li, *et al.*, "Numerical treatment of time dependent magnetohydrodynamic nanofluid flow of mass and heat transport subject to chemical reaction and heat source," *Alexandria Engineering Journal*, vol. 61, no. 3, pp. 2484–2491, 2022. DOI: 10.1016/j.aej.2021.07.030.

[12] R. Krechetnikov and G. M. Homsy, "On physical mechanisms in chemical reaction-driven tip-streaming," *Physics of Fluids*, vol. 16, no. 7, pp. 2556–2566, 2004. DOI: 10.1063/1.1739232.

[13] A. Kolin, "An electromagnetic flowmeter. principle of the method and its application to bloodflow measurements," Proceedings of the Society for Experimental Biology and Medicine 35(1), pp. 53–56, 1936. DOI: 10.3181/00379727-35-8854P.

[14] T. Kuwahara, F. De Vuyst and H. Yamaguchi, "Bubble velocity measurement using magnetic fluid and electromagnetic induction," *Physics of Fluids*, vol. 21, no. 9, pp. 097101, 2009. DOI: 10.1063/1.3213608.
[15] J. Yu, Z. Jiang, F. Liu, K. Chen, H. Li and X. Geng, "Effects of metal droplets on electromagnetic field, fluid flow and temperature field in electroslag remelting process," *ISIJ International*, vol. 57, no. 7, pp. 1205–1212, 2017. DOI: 10.2355/isijinternational.ISIJINT-2017-084.
[16] T. T. Natarajan and N. El-Kaddah, "Finite element analysis of electromagnetic and fluid flow phenomena in rotary electromagnetic stirring of steel," *Applied Mathematical Modelling*, vol. 28, no. 1, pp. 47–61, 2004. DOI: 10.1016/S0307-904X(03)00114-8.
[17] A. Chamkha, S. Abbasbandy and A. M. Rashad, "Non-Darcy natural convection flow for non-Newtonian nanofluid over cone saturated in porous medium with uniform heat and volume fraction fluxes," *Int. J. Numerical Methods Heat & Fluid Flow*, vol. 25, no. 2, pp. 422–437, 2015. DOI: 10.1108/HFF-02-2014-0027.
[18] B. Q. Li, "The fluid flow aspects of electromagnetic levitation processes," *International Journal of Engineering Science*, vol. 32, no. 1, pp. 45–67, 1994. DOI: 10.1016/0020-7225(94)90148-1.
[19] G. Ibáñez, A. López, J. Pantoja and J. Moreira, "Entropy generation analysis of a nanofluid flow in MHD porous microchannel with hydrodynamic slip and thermal radiation," *International Journal of Heat and Mass Transfer*, vol. 100, pp. 89–97, 2016. DOI: 10.1016/j.ijheatmasstransfer.2016.04.089.
[20] L. Zhang, M. M. Bhatti and E. E. Michaelides, "Electro-magnetohydrodynamic flow and heat transfer of a third-grade fluid using a Darcy-Brinkman-Forchheimer model," *HFF*, vol. 31, no. 8, pp. 2623–2639, 2021. DOI: 10.1108/HFF-09-2020-0566.
[21] S. M. Sachhin, M. S. Bharath, U. S. Mahabaleshwar, G. V. Bognar and L. M. Pérez, "Dual modeling of unsteady radiative non-Newtonian fluid flow with Biot boundary conditions using novel time-dependent solutions," *Mech Time-Depend Mater*, vol. 30, no. 1, pp. 5, 2026. DOI: 10.1007/s11043-025-09849-x.
[22] C. Dan and A. Wachs, "Direct numerical simulation of particulate flow with heat transfer," *Int. J. Heat Fluid Flow*, vol. 31, no. 6, pp. 1050–1057, 2010. DOI: 10.1016/j.ijheatfluidflow.2010.07.007.
[23] S. M. Sachhin, U. S. Mahabaleshwar, D. Laroze and L. M. Pérez, "Exact multiple solutions for rheological analysis of Darcy–Brinkman model on Bingham sodium alginate suspensions driven by 2D bidirectional moving plate with Navier and Biot conditions," *J Therm Anal Calorim*, vol. 150, no. 22, pp. 18327–18344, 2025. DOI: 10.1007/s10973-025-14693-9.
[24] S. Hoseinzadeh, P. S. Heyns and H. Kariman, "Numerical investigation of heat transfer of laminar and turbulent pulsating Al2O3/water nanofluid flow," *Int. J. Numerical Methods Heat & Fluid Flow*, vol. 30, no. 3, pp. 1149–1166, 2020. DOI: 10.1108/HFF-06-2019-0485.
[25] A. Dawar, S. Islam, Z. Shah and S. A. Lone, "A comparative analysis of the magnetized sodium alginate-based hybrid nanofluid flows through cone, wedge, and plate," *ZAMM - Journal of Applied Mathematics and Mechanics/Zeitschrift Für Angewandte Mathematik Und Mechanik*, vol. 103, no. 1, pp. e202200128, 2023.
[26] A. Dawar, S. Islam, Z. Shah and S. R. Mahmuod, "A passive control of Casson hybrid nanofluid flow over a curved surface with alumina and copper nanomaterials: a study on sodium alginate-based fluid," *Journal of Molecular Liquids*, vol. 382, pp. 122018, 2023. DOI: 10.1016/j.molliq.2023.122018.
[27] Himanshu, Upreti, J., Prakash, Alok Kumar, Pandey, Dharmendra, Tripathi, Usman, "Thermal analysis of 3D Darcy–Forchheimer flow of SWCNT–MWCNT/sodium alginate on Riga plate," *J Therm Anal Calorim*, vol. 149, no. 9, pp. 3891–3911, 2024. DOI: 10.1007/s10973-024-12975-2.
[28] S. Li, *et al.*, "Thermal attributes of sodium alginate (*Na.C6H7O6*) based binary and ternary hybrid nanofluids under activation energy and induced magnetic field environment," *Case Studies in Thermal Engineering*, vol. 59, pp. 104449, 2024. DOI: 10.1016/j.csite.2024.104449.
[29] T. K. Das, A. Paul and J. M. Nath, "Thermo-convection driven sodium alginate-based Darcy–Forchheimer EMHD Williamson hybrid nanofluid flow with varying thermal distribution," *Mod. Phys. Lett. B*, vol. 39, pp. 2450405, 2025. DOI: 10.1142/S0217984924504050.
[30] S. Chandrasekaran, M. Satyanarayana Gupta, S. Jangid, K. Loganathan, B. Deepa and D. K. Chaudhary, "Unsteady radiative maxwell fluid flow over an expanding sheet with sodium alginate water-based copper-graphene oxide hybrid nanomaterial: an application to solar aircraft," *Advances in Materials Science and Engineering*, vol. 2022, no. 1, pp. 1–16, 2022. DOI: 10.1155/2022/8622510.
[31] C.-H. Wang, Z.-Y. Liu, Z.-Y. Jiang and X.-X. Zhang, "Double-diffusive convection in a magnetic nanofluid-filled porous medium: development and application of a nonorthogonal lattice Boltzmann model," *Physics of Fluids*, vol. 34, no. 6, pp. 062012, 2022. DOI: 10.1063/5.0097330.
[32] E. H. Aly and A. Ebaid, "Exact analysis for the effect of heat transfer on MHD and radiation Marangoni boundary layer nanofluid flow past a surface embedded in a porous medium," *Journal of Molecular Liquids*, vol. 215, pp. 625–639, 2016. DOI: 10.1016/j.molliq.2015.12.108.
[33] M. Ameri and M. Seyd Eshaghi, "Exergy and thermal assessment of a novel system utilizing flat plate collector with the application of nanofluid in porous media at a constant magnetic field," *Thermal Science and Engineering Progress*, vol. 8, pp. 223–235, 2018. DOI: 10.1016/j.tsep.2018.08.004.

[34] E. H. Aly, "Existence of the multiple exact solutions for nanofluid flow over a stretching/shrinking sheet embedded in a porous medium at the presence of magnetic field with electrical conductivity and thermal radiation effects," *Powder Technology*, vol. 301, pp. 760–781, 2016. DOI: 10.1016/j.powtec.2016.06.024.

[35] H. Upreti, P. Bartwal, A. K. Pandey and O. D. Makinde, "Heat transfer assessment for Au-blood nanofluid flow in Darcy-Forchheimer porous medium using induced magnetic field and Cattaneo-Christov model," *Numerical Heat Transfer, Part B: fundamentals*, vol. 84, no. 4, pp. 415–431, 2023. DOI: 10.1080/10407790.2023.2209281.

[36] C. Luo, Y. A. Rothan, M. A. Alazwari, N. H. Abu-Hamdeh and M. M. Selim, "Multi-physics investigation within a porous media involving magnetic field impact on nanofluid," *Journal of Petroleum Science and Engineering*, vol. 207, pp. 109173, 2021. DOI: 10.1016/j.petrol.2021.109173.

[37] T. Fang and J. Zhang, "Closed-form exact solutions of MHD viscous flow over a shrinking sheet," *Commun. Nonlinear Sci. Numerical Simulation*, vol. 14, no. 7, pp. 2853–2857, 2009. DOI: 10.1016/j.cnsns.2008.10.005.

[38] W. K. Usafzai, E. H. Aly, A. S. Alshomrani and M. Z. Ullah, "Multiple solutions for nanofluids flow and heat transfer in porous medium with velocity slip and temperature jump," *Int. Commun. Heat Mass Transfer*, vol. 131, pp. 105831, 2022. DOI: 10.1016/j.icheatmasstransfer.2021.105831.

[39] U. Khan, *et al.*, "Exact solutions for MHD axisymmetric hybrid nanofluid flow and heat transfer over a permeable non-linear radially shrinking/stretching surface with mutual impacts of thermal radiation," *Eur. Phys. J. Spec. Top*, vol. 231, no. 6, pp. 1195–1204, 2022. DOI: 10.1140/epjs/s11734-022-00529-2.

[40] L. J. Crane, "Flow past a stretching plate," *Journal of Applied Mathematics and Physics (ZAMP)*, vol. 21, no. 4, pp. 645–647, 1970. DOI: 10.1007/BF01587695.

[41] K. B, "Pavlov, magnetohydrodynamic flow of incompressible viscous fluid caused by of a surface," *M. Gidrodinamika*, vol. 4, pp. 146–147, 1974.

[42] S. M. Sachhin, F.-J. Granados-Ortiz, U. S. Mahabaleshwar, J. Ortega-Casanova and L. M. Pérez, "Heat and mass transfer analysis of a Bingham ternary nanofluid exposed to radiation over stretching/shrinking sheets and Stefan blowing effect," *Alexandria Engineering Journal*, vol. 129, pp. 515–529, 2025. DOI: 10.1016/j.aej.2025.06.026.

[43] C. Zhao, Y. Liu, B. E. Hobbs, A. Ord and X. Zhang, "Theoretical investigation of boundary condition effects on chemical osmosis-induced water flow and solute concentration variation in a horizontal layer of the solution-saturated semi-permeable medium," *Transp Porous Med*, vol. 152, no. 9, pp. 62, Jul. 2025. DOI: 10.1007/s11242-025-02197-x.

[44] R. Snehashree, K. G. Chandan, P. Mallikarjun B and B. Souayeh, "Numerical and series solution for couple stress fluid flow in thermosolutal convection with soret and dufour effects," *Transp Porous Med*, vol. 152, no. 9, pp. 68, 2025. DOI: 10.1007/s11242-025-02205-0.

[45] A. Thakur, S. Kumar and R. Devi, "Modeling heat transfer in rotating ferrofluids with couple stresses under local thermal non-equilibrium using ANN," *Transp Porous Med*, vol. 152, no. 9, pp. 1–31, 2025. DOI: 10.1007/s11242-025-02204-1.

[46] C. Bringedal, S. Kiemle, C. J. van Duijn and R. Helmig, "Impact of saturation on evaporation-driven density instabilities in porous media: mathematical and numerical analysis," *Transp Porous Med*, vol. 152, no. 10, pp. 72, 2025. DOI: 10.1007/s11242-025-02207-y.

[47] A. Mahajan and S. P, "Convective heat transfer in Brinkman–Darcy–Kelvin–Voigt fluid with variable gravity and generalized maxwell-Cattaneo law," *Transp Porous Med*, vol. 152, no. 8, pp. 55, 2025. DOI: 10.1007/s11242-025-02194-0.

[48] R. Kumar, N. Sharma and V. Rani, "A comprehensive examination of fundamental solution and Green's function in orthotropic photothermoelastic media including moisture," *J. Thermal Stresses*, vol. 49, no. 4, pp. 527–559, 2026. DOI: 10.1080/01495739.2025.2575045.

[49] H. Zougheib, T. El Arwadi, R. L. R. Madureira, M. A. Rincon and T. Sayah, "Exponential stability of a fully discrete energy associated to a thermoviscoelastic Timoshenko system," *J. Thermal Stresses*, vol. 49, no. 5, pp. 635–650, 2026. DOI: 10.1080/01495739.2025.2574703.

[50] S. M. Sachhin, U. S. Mahabaleshwar, N. Swaminathan, L. M. Pérez and J. Wang, "Thermal dynamics and magnetohydrodynamics in ferrofluidic wall jet flow: entropy generation in heat and mass transfer," *Journal of Molecular Liquids*, vol. 427, pp. 127449, 2025. DOI: 10.1016/j.molliq.2025.127449.

[51] S. Singh and R. Nandkeolyar, "Modeling blood flow with tetra-hybrid Casson nanofluid in stenosed arteries: numerical and machine learning approach," *J. Thermal Stresses*, vol. 49, no. 4, pp. 570–598, 2026. DOI: 10.1080/01495739.2025.2578599.

[52] M. Sohail, N. Jabbar, W. Sumelka and U. Nazir, "Numerical analysis of thermal enhancement induced by partially ions suspended in co-axially swirled disks," *J. Thermal Stresses*, vol. 48, no. 12, pp. 1746–1770, 2025. DOI: 10.1080/01495739.2025.2499052.

[53] I. Bochicchio, A. Sellitto and C. F. Munafó, "Phonon-boundary scattering and second-order boundary conditions: application to the heat transfer in one-dimensional nanosystems," *J. Thermal Stresses*, vol. 48, no. 12, pp. 1568–1583, 2025. DOI: 10.1080/01495739.2025.2458724.

[54] U. S. Mahabaleshwar, S. M. Sachhin, R. Ragoju, D. Laroze and G. V. Bognar, "Mathematical modelling of waste discharge and irreversible mechanism impact on chemically reactive electromagnetic Maxwell fluid suspensions driven by Darcy–Forchheimer structures with thermo-solutal transfer," *J Therm Anal Calorim*, vol. 151, no. 4, pp. 3607–3620, 2026. DOI: 10.1007/s10973-026-15289-7.

[55] A. M. Al-Mahdi, M. Aouadi and M. M. Al-Gharabli, "Stability of thermoelastic extensible Timoshenko system with nonlinear frictional damping of variable exponent-type," *J. Thermal Stresses*, vol. 49, no. 2, pp. 149–166, 2026. DOI: 10.1080/01495739.2025.2519939.

[56] P. Kumar and R. Prasad, "Thermoelastic damping on micromechanical resonators under HTTMGT thermoelasticity," *J. Thermal Stresses*, vol. 49, no. 2, pp. 193–206, 2026. DOI: 10.1080/01495739.2025.2578597.

[57] G. Bognár and K. Hriczó, "Ferrofluid flow in magnetic field above stretching sheet with suction and injection," *Math. Modelling Anal.*, vol. 25, no. 3, pp. 461–472, 2020. DOI: 10.3846/mma.2020.10837.

[58] M. Waseem, E. A. Algehyne, N. O. Al-Atawi, G. Bognár, M. Jawad and S. Naeem, "Non-similar analysis of suction/injection and Cattaneo-Christov model in 3D viscoelastic non-Newtonian fluids flow due to Riga plate: a biological applications," *Alexandria Engineering J.*, vol. 103, pp. 121–136, 2024. DOI: 10.1016/j.aej.2024.05.099.

[59] E. A. Algehyne, F. M. Alamrani, M. M. Seada, A. Saeed and G. Bognár, "Numerical examination of the chemically reactive MHD flow of hybrid nanofluids over a two-dimensional stretching surface with the Cattaneo–Christov model and slip conditions," *Open Physics*, vol. 23, pp. 20250140, 2025. DOI: 10.1515/phys-2025-0140.